An inverse strategy to determine constitutive parameters of tubular materials for hydroforming processes

ZHANG, Bin; ENDELT, Benny; LANG, Lihui; ZHAO, Yang; YAN, Shu; NIELSEN, Karl Brian

Published in:
Chinese Journal of Aeronautics

DOI (link to publication from Publisher):
10.1016/j.cja.2021.11.007

Publication date:
2022

Document Version
Publisher's PDF, also known as Version of record

Chinese Journal of Aeronautics, (2022), 35(6): 379–390

Chinese Society of Aeronautics and Astronautics
& Beihang University

Chinese Journal of Aeronautics

cja@buaa.edu.cn
www.sciencedirect.com

An inverse strategy to determine constitutive parameters of tubular materials for hydroforming processes

Bin ZHANG [a,*], Benny ENDELT [a], Lihui LANG [b], Yang ZHAO [c], Shu YAN [c], Karl Brian NIELSEN [d]

[a] *Department of Materials and Production, Aalborg University, Aalborg 9220, Denmark*
[b] *School of Mechanical Engineering and Automation, Beihang University, Beijing 100083, China*
[c] *School of Materials Science and Engineering, Northeastern University, Shenyang 110819, China*
[d] *Department of Mechanical and Production Engineering, Aarhus University, Aarhus 8000, Denmark*

Received 20 February 2021; revised 29 March 2021; accepted 2 June 2021
Available online 22 November 2021

KEYWORDS

Aluminum alloy;
Constitutive parameter;
Hydraulic bulging test;
Inverse modelling;
Tubular material

Abstract This paper is to determine the flow stress curve of 5049-O aluminium alloy by a tube hydraulic bulging test with fixed end-conditions. During this test, several tubular specimens are bulged under different internal pressures before their bursting, and the corresponding bulging height and wall thickness at the pole are measured. An inverse strategy is developed to determine the constitutive parameters of tubular materials based on experimental data, which combines the finite element method with gradient-based optimization techniques. In this scheme, the objective function is formulated with the sum of least squares of the error between numerical and experimental data, and finite difference approximation is used to calculate the gradient. The tubular material behavior is assumed to meet the von Mises yield criterion and Hollomon exponential hardening law. Then, constitutive parameters identification is performed by minimization of the objective function. In order to validate the performance of this framework, identified parameters are compared with those obtained by two types of theoretical models, and tensile tests are performed on specimens cut from the same tubes. The comparison shows that this inverse framework is robust and can achieve a more accurate parameter identification by eliminating mechanical and geometrical assumptions in classical theoretical analysis.

* Corresponding author.
E-mail address: zb@m-tech.aau.dk (B. ZHANG).
Peer review under responsibility of Editorial Committee of CJA.

1. Introduction

Tube hydroforming technology has been proven to be a successful manufacturing process and can form tubular metal blanks into various complex tube components. Such a forming process is widely utilized in the aviation and aerospace indus-

https://doi.org/10.1016/j.cja.2021.11.007
1000-9361 © 2021 Chinese Society of Aeronautics and Astronautics. Production and hosting by Elsevier Ltd.

try[1] owing to its advantages such as weight reduction, increase of part complexity, and cost savings.[2] A robust and productive hydroforming process depends heavily on several process parameters like incoming tubular material, preforming operation, fluid pressure loading path, lubrication, equipment, and tools. Among the above factors, materials properties, i.e. the flow stress curve and the tool-workpiece friction, have drastic influences on the quality of final hydroformed parts. Besides, an accurate evaluation of incoming tube material properties is essential for the input data in the Finite Element Method (FEM).[3]

To determine tubular metal properties, a number of industrial tests have been carried out to measure material behaviors. One of the simplest methods is the tensile test which is used to test sheet metal behaviors commonly.[4] When it is applied on a tubular material, specimens can be cut from the tube wall at different locations along the longitudinal and circumferential directions, and then will be flattened and tested under uniaxial tension according to the ASTM standard.[5] However, the flattening process of curved specimens before testing will change their strain–stress behaviors and formability, especially those cut from small-diameter tubes. The ring hoop tensile test can avoid the unnecessary work hardening caused by flattening and measure the hoop flow stress curve of a tubular material accurately. In this test, a ring specimen with a reduced section is taken from a tube along the hoop direction and then pulled by a universal tensile apparatus. A disadvantage of this method is the friction on the interface between the specimen and a pair of blocks, which will lead to some measuring errors.[6]

Another more accurate method to measure tubular material properties is the hydraulic bulge test, because the stress state of specimens under this procedure is close to the realistic hydroforming process. A number of efforts have been made to various types of hydraulic bulge testing methods and post-processing procedures for experimental data. Fuchizawa et al.[7] ignored the stress through thickness and calculated stress components along circumferential and longitudinal directions based on the recorded internal pressure, wall thickness, and bulge height near the tube center in experiments. The use of three displacement sensors to improve the accuracy of measuring the meridian profile shape increased the complexity and cost of the hydraulic press. Hwang et al.[8] proposed a simple analytical model where the bugle profile shape was assumed as an elliptical curve to avoid measuring the longitudinal curve radius, and the flow stress curve could be obtained when only the tube center diameter and pole thickness were measured.

Other studies on theoretical analysis for the hydro bulge process are similar, in which they followed the same stress formulas as those of Hwang et al.[8] and Fuchizawa et al.[7] and only changed the shape assumption. The meridian profile shape could be assumed as two circular arcs,[9] spline functions.[10] However, to calculate the axial stress component, those researchers adopted an unreasonable hypothesis that tubular specimens and dies were regarded as a whole and isolated the analyses for stress and strain. Bortot et al.[11] introduced a plastic strain–stress relationship, i.e. strain components were proportional to the corresponding deviatoric stress to derive the longitudinal stress component while the tube thickness was ignored in the radical force equilibrium equation for a pole element. In all the above analytical approaches, the tube deformation was treated as a plane stress problem, and the tube bulge profile was assumed as a simple mathematical formula; this simplicity reduced the accuracy of results to some extent.

A substantial progress for the identification material parameters of analytical models is the application of the inverse modelling strategy which combines the optimization technique with the FEM model and obtains the optimum material coefficients by minimizing the difference between numerical simulation results and experimental data. Compared with the classical theoretical equations, it allows a more accurate determination by avoiding mechanical and geometrical assumptions.[12] A large number of publications focused on the inverse identification of sheet metal properties,[13–17] and limited work was carried out on the application of inverse modelling on the tube hydraulic bulge test. Zribi et al.[18,19] used this inverse procedure combining the FEM with Nelder Mead simplex algorithm to identify material constitutive parameters of tubular parts made of low carbon steel. The gap of the internal pressure versus the bulge curve between collected from a free hydraulic bulging experiment and FEM responses was set as the cost function. One limitation of this research was that the direct search algorithm in the strategy showed a lower efficiency and a lack of comparison with classical theoretical analysis.

In this paper, a novel and flexible hydraulic setup is designed, and several tube hydraulic tests with fixed end-conditions for annealed 5049 aluminium alloy are carried out. The bulge height, wall thickness at the pole, and applied internal pressure are measured during the process. An inverse modelling technique combining the FEM model and an improved Levenberg-Marquardt algorithm is used to determine the tubular materials constitutive parameters of 5049-O aluminium alloy. A general objective function is created to evaluate the difference between computed and experimental data, and material constitutive parameters are identified by minimizing this function. Meanwhile, two theoretical models based on the force equilibrium and total strain theory for this process are given, and tensile tests for specimens cut from the tube along the longitudinal direction are performed. In order to demonstrate the inverse strategy's feasibility and performance, a comparison of three types of methods is carried out by running FEM simulation of the tube hydraulic bulging process.

2. Hydraulic bulging test analysis

A tube hydraulic bulging test is a material characterization method which expands a tubular material into a suitable shape freely using the internal fluid pressure. In the test, some data such as the bulge height, internal pressure, and pole thickness can be measured online or offline, and then these collected data can be used further to determine tubular material properties. Fig. 1 illustrates a typical tube hydraulic bulging process. In general, this test includes three types of end-conditions at tube ends: A) Free-end, B) Forced-end, and C) Fixed-end; the ends of a tubular workpiece are fixed completely in current study.

2.1. Geometrical analysis

The profile of the deformation zone on a tube is assumed as an elliptical curve.[8] The geometrical parameters for this shape are shown in Fig. 2, where R_0 is the initial external tube radius, t_0

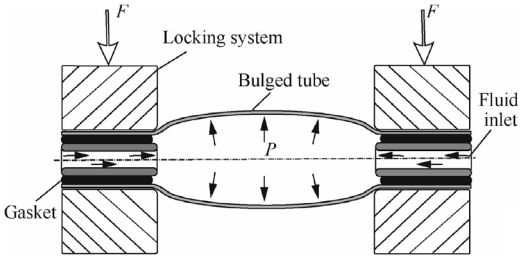

Fig. 1 Schematic for tube hydraulic bulging process.

is the initial tube wall thickness, L_0 is the length of the bulge zone, h is the bulge height. The elliptical curve can be defined as[20]

$$\frac{z^2}{a^2}+\frac{r^2}{b^2}=1 \tag{1}$$

where a and b are the half lengths of the major and minor axes of the ellipse, respectively.

In Fig. 2, it can be seen that the coordinates of the contact point between the tube and the die are $(L_0/2, R_0)$, and the elliptical curve passes through this point. The pole point $(0, R_0 + h)$ also meets Eq. (1), and then parameters a and b in the elliptical equation can be determined as[20]

$$a=\frac{L_0(R_0+h)}{\sqrt{4h(2R_0+h)}} \tag{2}$$

$$b=R_0+h \tag{3}$$

Based on Eqs. (1)–(3), the meridian curvature radius at the pole point can be described as[20]

$$r_\varphi=\frac{L_0^2(R_0+h)}{4h(2R_0+h)} \tag{4}$$

Then, the circumferential radius at the pole of the tube bulge zone can be written as

$$r_\theta=R_0+h \tag{5}$$

As a comparison, Hwang et al.[8] applied another elliptic shape equation to describe the profile, and r_φ can be calculated as

$$r_\varphi=\frac{a^2}{b} \tag{6}$$

It can be seen from Eq. (1)–(6) that the meridian and circumferential radii depend on the bulge height, tube thickness, and diameter, which can be measured during the hydraulic bulging test.

2.2. Stress analysis

For the thin-walled tube used in this research, the ratio of its thickness to diameter $\ll 1$, so the stress within the workpiece can be referred as the plane stress state according to assumptions in the membrane theory. It means that the stress along the thickness direction is zero, i.e.

$$\sigma_t=0 \tag{7}$$

The equivalent stress can be calculated by two stress components, σ_θ along the circumferential direction and σ_φ along the longitudinal direction. They can be determined from the force equilibrium along the thickness direction for a membrane element at the pole of the tube bulge zone, as shown in Fig. 3, which can get

$$\begin{aligned}&2\sigma_\varphi(r_\theta-\frac{t}{2})t\theta\sin\frac{\varphi}{2}+2\sigma_\theta(r_\varphi-\frac{t}{2})t\varphi\sin\frac{\theta}{2}\\&=P(r_\theta-t)\varphi(r_\varphi-t)\theta\cos\frac{\theta}{2}\sin\frac{\varphi}{2}\end{aligned} \tag{8}$$

where r_θ and r_φ are the circumferential and meridian curve radii at a point of the tubular elliptical surface, respectively; P is the internal fluid pressure; θ and φ are the angles on the planes of hoop and meridian, respectively. When these angles are small, Eq. (8) can be rewritten as[20]

$$\frac{\sigma_\varphi}{r_\varphi-\frac{t}{2}}+\frac{\sigma_\theta}{r_\theta-\frac{t}{2}}=\frac{P(r_\theta-t)(r_\varphi-t)}{t(r_\theta-\frac{t}{2})(r_\varphi-\frac{t}{2})} \tag{9}$$

According to Fuchizawa et al.[7] and Hwang et al.,[8] the hypothesis that both ends of the tube were considered closed was applied. For a closed tube under internal pressure, from the force equilibrium equation along the longitudinal direction at the cross-section perpendicular to the tube surface, it can be expressed as[21]

$$2\pi\left(r_\theta-\frac{t}{2}\right)t\sigma_\varphi=P\pi(r_\theta-t)^2 \tag{10}$$

Based on hypothesis Eq. (10), the longitudinal stress at the pole can be approximately calculated as[8]

$$\sigma_\varphi=\frac{P(r_\theta-t)^2}{2t(r_\theta-\frac{t}{2})} \tag{11}$$

Substituting Eq. (11) into Eq. (9), the stress along the hoop direction can be written as[8]

$$\sigma_\theta=\frac{P(r_\theta-t)}{2t(r_\varphi-\frac{t}{2})}(2r_\varphi-t-r_\theta) \tag{12}$$

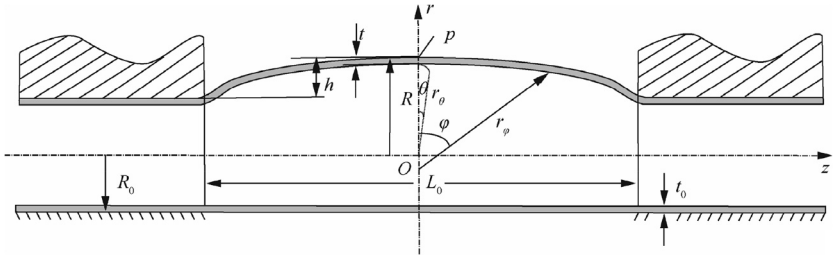

Fig. 2 Tube geometrical parameters before and after bulging test.

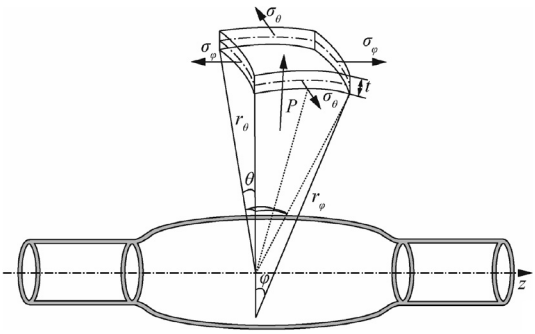

Fig. 3 Stress state of a small element at tube pole.

The other method to calculate the stress along the longitudinal direction is presented based on the total strain theory proposed by Ilyushin and Lensky.[22] During the test, the internal fluid pressure increases continuously without intermediate unloading. The Ilyushin plastic strain–stress relationship can be expressed by

$$\sigma_\varphi' = \frac{2}{3}\frac{\sigma_{\text{eff}}}{\varepsilon_{\text{eff}}}\varepsilon_\varphi' \tag{13}$$

$$\sigma_t' = \frac{2}{3}\frac{\sigma_{\text{eff}}}{\varepsilon_{\text{eff}}}\varepsilon_t' \tag{14}$$

$$\sigma_\theta' = \frac{2}{3}\frac{\sigma_{\text{eff}}}{\varepsilon_{\text{eff}}}\varepsilon_\theta' \tag{15}$$

where $\boldsymbol{\sigma}' = [\sigma_\varphi', \sigma_t', \sigma_\theta']$ and $\boldsymbol{\varepsilon}' = [\varepsilon_\varphi', \varepsilon_t', \varepsilon_\theta']$ are the stress and strain deviators at a certain deformation state, respectively; σ_{eff} is the effective stress; ε_{eff} is the effective strain. Considering the total stress, Eq. (16) can be derived:

$$\frac{\sigma_\varphi - \sigma_t}{\varepsilon_\varphi - \varepsilon_t} = \frac{\sigma_t - \sigma_\theta}{\varepsilon_t - \varepsilon_\theta} = \frac{\sigma_\theta - \sigma_\varphi}{\varepsilon_\theta - \varepsilon_\varphi} \tag{16}$$

where ε_φ, ε_t and ε_θ are the strains along longitudinal, thickness and circumferential directions.

Combination Eq. (16) with Eq. (9), the stress along the circumferential direction can be obtained as

$$\sigma_\theta = \frac{P(r_\varphi - t)(r_\theta - t)}{(\varepsilon_t - \varepsilon_\varphi)(r_\theta - \frac{t}{2}) + (\varepsilon_t - \varepsilon_\theta)(r_\varphi - \frac{t}{2})} \tag{17}$$

The stress along the longitudinal direction can be derived from Eq. (9) as

$$\sigma_\varphi = \frac{P(r_\theta - t)(r_\varphi - t) - \sigma_\theta t(r_\varphi - \frac{t}{2})}{t(r_\theta - \frac{t}{2})} \tag{18}$$

From Eqs. (7)–(18), the application of the plane stress state assumption ignores the stress through the thickness and simplifies the calculation for the stress tensor at the tube pole. Classical Hwang model and total strain model are presented to calculate the other two stress components along the longitudinal and circumferential directions, respectively. Whichever method is used, it is essential to measure the bulge height and pole thickness during the test.

The tube is assumed as an isotropic material and meets von Mises yield criterion, so its effective stress can be expressed by

$$\sigma_{\text{eff}} = \frac{1}{\sqrt{2}}\sqrt{(\sigma_\theta - \sigma_t)^2 + (\sigma_t - \sigma_\varphi)^2 + (\sigma_\varphi - \sigma_\theta)^2} \tag{19}$$

where σ_t, σ_θ and σ_φ can be obtained using Eqs. (7), (17), (18).

2.3. Strain analysis

For a calculation of the strain tensor at the pole point, assume that the strain increment is continuous and the principal strain direction keeps identical during the test. Thus, the strains along the circumferential and thickness directions can be described as[7]

$$\varepsilon_\theta = \ln\frac{R_0 + h - \frac{t}{2}}{R_0 - \frac{t_0}{2}} \tag{20}$$

$$\varepsilon_t = \ln\frac{t}{t_0} \tag{21}$$

Based on the volume constancy condition, the strain component ε_φ in the longitudinal direction can be written as

$$\varepsilon_\varphi = -(\varepsilon_\theta + \varepsilon_t) \tag{22}$$

In the bulge test, the internal fluid pressure increases continuously, and no intermediate unloading occurs. Tubular metal meets von Mises yield criterion, and the associated isotropic hardening model is considered to represent the subsequent yield surface; thus, the effective strain can be derived as

$$\varepsilon_{\text{eff}} = \frac{\sqrt{2}}{3}\sqrt{(\varepsilon_\theta - \varepsilon_t)^2 + (\varepsilon_t - \varepsilon_\varphi)^2 + (\varepsilon_\varphi - \varepsilon_\theta)^2} \tag{23}$$

3. Inverse strategy

The inverse modelling technique can be used to explore the optimum process design and identify material constitutive parameters. In general, an establishment process of inverse schemes involves the following steps: (A) Problem statement and FEM modelling; (B) Definition of design variables, objective functions, and constraints; (C) Data collection and solution for the optimization problem; (D) Evaluation of potential optimum parameters. Fig. 4 illustrates the flow chart of the inverse framework applied to determine constitutive parameters of tubular materials. The key steps mentioned above will be elaborated separately.

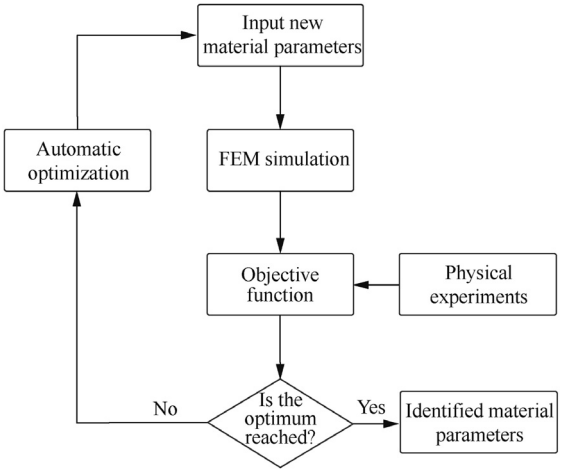

Fig. 4 Flow chart of inverse framework used for parameters identification of tubular materials.

3.1. FEM modelling of tube bulging process

The FEM model for the tube bulge process is created by general-purpose programme LS-DYNA, which is shown in Fig. 5. In this model, the tube is meshed by three-dimensional solid elements with eight-node hexahedrons, and three elements are produced through the tube wall thickness for an accurate response. Tubes used in the experiment are annealed, and the holding time lasts for 3 h, which means that the material has a strong isotropy. The von Mises yield criterion and Hollomon isotropic hardening law are used to describe the tubular materials' mechanical behaviors.

The internal fluid pressure is referred to as the compression stress and applied on the inner wall of the tube along the radial direction, and the pressure curve follows the one collected from the experiment. In order to reduce the calculation time, the mass scaling strategy is used, and a half of the tube is selected as the FEM model. Tube ends are fixed at all translational and rotational directions, because there is no sliding between tubes and the locking system by observation and measurement during the test.

3.2. Objective function and design variables

The nature of an inverse analysis is an optimization problem where design variables, i.e. material mechanical coefficients, are identified by minimizing the objective function under specified constraints. The material response under plastic deformation can be described by variety of constitutive equations with mathematical coefficients which will also be imported into FEM models easily. Therefore, the objective of the inverse analysis is to find the material parameters in the constitutive models, and the design variables can be defined as

$$\boldsymbol{x} = [x_1, x_2, ..., x_n]^{\mathrm{T}} \tag{24}$$

where n is the number of coefficients in the material model, and x_j is the j th element in this vector. To characterize tubular material mechanical properties with unknown design variables, a common elastic–plastic model with power law isotropic hardening is used to describe its behavior where the flow stress equation can be expressed as

$$\sigma_{\mathrm{eff}} = K\varepsilon_{\mathrm{eff}}^{e} \tag{25}$$

where K is the strength coefficient; e is the hardening exponent, and these two material parameters can be selected as design variables.

The objective function is a pointer to evaluate the error between experimental and simulated data, which should have the following properties:[23]

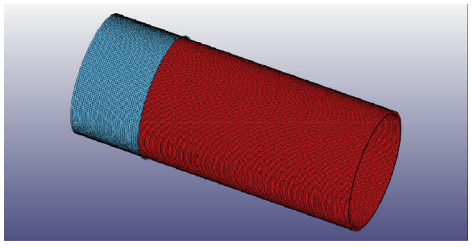

Fig. 5 FEM model for hydraulic bulging process.

(1) All collected experimental data using different methods and equipment should be involved in the iteration process.
(2) The final optimization results should not be sensitive to the unit of the data.
(3) Weighting factors need to be allocated to different experimental points according to their physical characteristics.

In the tube hydraulic bulge test, the filling height and pole thickness under different internal pressures are collected, so the cost function should consist of the above two terms. Meanwhile, an error definition with a least square structure is introduced to increase the sensitivity of the cost function to the design variables and reduce the influences of the two measure indicators' magnitudes.[24] Therefore, the objective function can be defined as

$$f = \alpha f_1 + (1-\alpha) f_2 \tag{26}$$

$$f_1 = \sum_{i_1=1}^{n_1} [\omega_{i_1}(h_{i_1}^{\exp} - h_{i_1}^{\mathrm{sim}})]^2 \tag{27}$$

$$f_2 = \sum_{i_2=1}^{n_2} [\omega_{i_2}(t_{i_2}^{\exp} - t_{i_2}^{\mathrm{sim}})]^2 \tag{28}$$

where f_1 is the first part in the cost function for representing the residual of the bulge height h under different pressures; f_2 is the second residual of the pole thickness t obtained by simulations and experiments; α is a weighted factor ranging from 0 to 1 to represent the importance of the two sub-objectives of the cost function; the subscript i_1 and i_2 represent the i_1 th data point of the bulge height and the i_2 th data point of the pole thickness, respectively; the superscript exp and sim represent the data point of experiment and simulation; n_1 and n_2 are the total experimental point numbers for the pole thickness and bulge height, respectively; ω is an automatic scaling factor to increase the sensitivity of experimental points especially in the area of large plastic deformation for the two sub-objective functions, and can be expressed as[24]

$$\omega_{i_1} = \frac{2(n_1+n_2)h_{i_1}^{\exp}}{\sum_{i_1=1}^{n_1}\sum_{i_2=1}^{n_2}(h_{i_1}^{\exp} + t_{i_2}^{\exp})} \tag{29}$$

The scaling factor ω_{i_1} calculated by Eq. (29) can be distributed to the corresponding residuals in the first sub-objective function. ω_{i_2} can be obtained by a similar formula to Eq. (29) and is used for the second sub-objective function.

3.3. Optimization algorithm

The inverse parameter identification can be seen as an optimization problem, so an efficient and robust optimization method is necessary to minimize the defined cost function in Eq. (26). A classical and robust gradient-based optimization method, i.e. an improved Levenberg-Marquardt algorithm is used to identify the tubular mechanical parameters.

As can be seen from Eqs. (26)–(29), the objective function consists of the sum of the squares of the true errors between experimental and simulated responses and can be regarded as a nonlinear least square problem. The Gauss-Newton method with line search performs very poorly and leads to

numerical convergence difficulties, because the true error, i.e. the residual function $\boldsymbol{r}(\boldsymbol{x})$ including the FEM model, exhibits severe nonlinearity. In order to overcome these difficulties, an improved Levenberg-Marquardt algorithm with the trust region strategy is considered where the objective function can be approximated as a quadratic model in the neighborhood of a given starting point $\boldsymbol{x}_k$ as

$$\boldsymbol{f}(\boldsymbol{x}_k+\boldsymbol{s}_k)\simeq\bar{\boldsymbol{f}}(\boldsymbol{s}_k)=\boldsymbol{f}(\boldsymbol{x}_k)+\boldsymbol{g}^{\mathrm{T}}(\boldsymbol{x}_k)\boldsymbol{s}_k+\frac{1}{2}\boldsymbol{s}_k^{\mathrm{T}}\boldsymbol{G}(\boldsymbol{x}_k)\boldsymbol{s}_k \tag{30}$$

where $\boldsymbol{x}_k$ is design variable at k th iteration; $\boldsymbol{s}_k$ is step size; $\boldsymbol{g}(\boldsymbol{x}_k)$ and $\boldsymbol{G}(\boldsymbol{x}_k)$ are the gradient and Hessian matrix of the cost function, respectively, which can then be expressed as

$$\boldsymbol{g}(\boldsymbol{x}_k)=\boldsymbol{J}^{\mathrm{T}}(\boldsymbol{x}_k)\boldsymbol{r}(\boldsymbol{x}_k) \tag{31}$$

$$\boldsymbol{G}(\boldsymbol{x}_k)=\boldsymbol{J}^{\mathrm{T}}(\boldsymbol{x}_k)\boldsymbol{J}(\boldsymbol{x}_k)+\boldsymbol{S}(\boldsymbol{x}_k) \tag{32}$$

where $\boldsymbol{S}(\boldsymbol{x}_k)$ is second term in the Hessian matrix; $\boldsymbol{J}(\boldsymbol{x}_k)$ is Jacobian matrix of the cost function.

The Jacobian matrix $\boldsymbol{J}(\boldsymbol{x}_k)$ is the first partial derivatives of the residual function $\boldsymbol{r}(\boldsymbol{x})$. It is impossible to give an analytical formula for Jacobian $\boldsymbol{J}(\boldsymbol{x}_k)$, because $\boldsymbol{f}(\boldsymbol{x})$ is a nonlinear implicit function and given in a black box. Therefore, the finite difference strategy is introduced to calculate the (i, j) th element in Jacobian matrix $\boldsymbol{J}(\boldsymbol{x}_k)$ by

$$\frac{\partial \boldsymbol{r}_i}{\partial \boldsymbol{x}_j}=\frac{\boldsymbol{r}_i(\boldsymbol{x}_k+\delta\boldsymbol{e}_j)-\boldsymbol{r}_i(\boldsymbol{x}_k)}{\delta} \tag{33}$$

where $\boldsymbol{r}_i$ is the i th component of objective function; δ is chosen appropriately small; $\boldsymbol{e}_j$ is the unit vector. Then the step size $\boldsymbol{s}_k$ can be defined by the solution of Eqs. (30)–(33) using the trust region technique as

$$\boldsymbol{x}_{k+1}=\boldsymbol{x}_k-(\boldsymbol{J}^{\mathrm{T}}(\boldsymbol{x}_k)\boldsymbol{J}(\boldsymbol{x}_k)+\boldsymbol{S}(\boldsymbol{x}_k))\boldsymbol{g}(\boldsymbol{x}_k) \tag{34}$$

$$\boldsymbol{S}(\boldsymbol{x}_k)=\mu_k\boldsymbol{D}_k^{\mathrm{T}}\boldsymbol{D}_k \tag{35}$$

where μ_k is damping factor; $\boldsymbol{D}_k$ is the diagonal and positive definite matrix.

The damping factor μ_k can be used to control the searching direction and step size in the current iteration. A new update strategy for the value of μ_k is recommended and numerical experiments demonstrate its good robustness and smoothness.[25] The change of μ_k depends on the gain ratio ρ which indicates the agreement of the approximated function to the actual objective function and can be written as

$$\rho=\frac{\|\boldsymbol{r}(\boldsymbol{x}_k)\|^2-\|\boldsymbol{r}(\boldsymbol{x}_k+\boldsymbol{s}_k)\|^2}{\|\boldsymbol{r}(\boldsymbol{x}_k)\|^2-\|\boldsymbol{r}(\boldsymbol{x}_k)+\boldsymbol{J}(\boldsymbol{x}_k)\boldsymbol{s}_k\|^2} \tag{36}$$

A wide variation of values between the strength coefficient and the hardening exponent could be of order 10^4. The ellipsoidal trust region[26] is used to reduce the effects of poor scaling in inverse problems, where a diagonal and positive definite matrix $\boldsymbol{D}_k$ is introduced into this formula, of which diagonal entries can be updated from iteration to iteration by

$$\boldsymbol{D}_k=\mathrm{diag}\left(d_1^k,d_2^k,\cdots,d_{n_1+n_2}^k\right) \tag{37}$$

$$d_i^0=\left\|\frac{\partial \boldsymbol{r}_i(\boldsymbol{x}_0)}{\partial \boldsymbol{x}_0}\right\| \tag{38}$$

$$d_i^k=\max\left(d_i^{k-1},\left\|\frac{\partial \boldsymbol{r}_i(\boldsymbol{x}_k)}{\partial \boldsymbol{x}_k}\right\|\right)\quad k\geq 1 \tag{39}$$

The new point $\boldsymbol{x}_{k+1}$ can be updated iteration by iteration using the solution of Eq. (34). Then, the optimum point will be obtained when the optimization process meets the convergence conditions. Therefore, two stopping criteria are used in this algorithm:

$$\|\boldsymbol{g}(\boldsymbol{x}_k)\|\leq\delta_1 \tag{40}$$

$$\|\boldsymbol{x}_{k+1}-\boldsymbol{x}_k\|\leq\delta_2(\|\boldsymbol{x}_k\|+\delta_2) \tag{41}$$

where δ_1 and δ_2 are two small and positive real numbers given by a user. When these two criteria are satisfied, the iteration process will be terminated.

4. Experimental tooling and method

4.1. Tensile test

A standard uni-axial tensile test has been conducted to characterize the flow stress curve of used tubular aluminium tubes. Tensile specimens are cut directly from the tubes along the longitudinal direction as shown in Fig. 6, and their geometric dimensions follow the ASTM E8/E8M-21 standard.[5] However, the subsize specimen type is used for the tensile test, because the diameter of the tubes is so small that standard tensile specimens are difficult to be machined. The tensile test is performed at room temperature and under a strain rate of 1.4 mm/min using a CMT electrical universal testing machine.

4.2. Hydraulic bulge test

A flexible tube hydraulic bulging device has been designed and manufactured to determine the tubular material flow strain–stress behavior under the bi-axial stress state, as shown in Fig. 7. It can be seen that this setup is mainly comprised of a hydraulic power system, a control system, and basic die sets. The two outermost hydraulic cylinders can not only move on the basement horizontally and achieve more flexibility for testing tubes with different lengths, but also apply an axial force or even a stretch force on tube ends and produce different stress states for specimens during a test.

Tube ends could be locked by two hydraulic clamping devices in the middle to guarantee no sliding along the axial

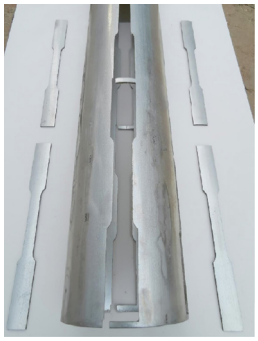

Fig. 6 Specimens for tensile test cut from tube along longitudinal direction.

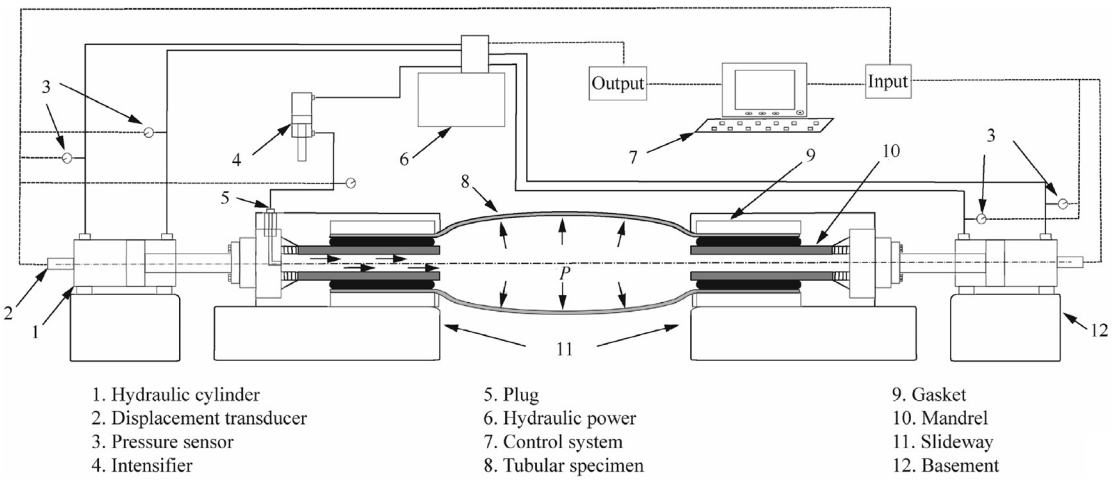

Fig. 7 Schematic diagram for hydraulic bulging setup.

direction of specimens and fluid leakage. By changing the mandrels and gaskets in the locking system, tubes with different diameters and wall thicknesses can be tested. Fig. 8 illustrates the schematic diagram of this flexible locking setup.

Bulging tests of annealed aluminium alloy tubes are performed on this hydraulic machine. The maximum bulging pressure is determined firstly by a general tube bulge until its bursting, and this procedure is repeated at least three times to get an accurate average bursting value. Then several tubular specimens are formed under different pressure levels lower than the maximum bursting pressure. After the bulging pressure reaches to a specified value, the tube is taken off from the machine. The bulge height and pole thickness can be measured by a micrometer, and the corresponding internal pressure is recorded by a transducer on the machine.

5. Results and discussion

Fully-annealed 5049 aluminium seamless tubes are used and investigated, of which chemical compositions are displayed in Table 1. The initial diameter and wall thickness of tested samples are 50.00 mm and 1.086 mm, respectively. The total length of every tubular specimen in the hydraulic bulge test is 300.00 mm, and the bulge zone is about 243.00 mm long.

The maximum bulging pressure is 7.8 MPa determined by the observation of the first tubular specimen bursting. Below this pressure value, more tube hydraulic bulging tests are performed under different pressure levels. To obtain more equivalent strain–stress points, 16 pressure levels with distinct intervals are inserted into the reasonable range. After the bulging, the corresponding bulge height and wall thickness at the tube pole are measured every 90° along the tube circumferential direction in the middle cross-section of the bulged tube, and several recorded typical values are displayed in Table 2. It is obvious that with an increase of the internal pressure, the diameter of the tube is increased, and the pole thickness becomes thinner.

Fig. 9 shows the profile shape of all tubular specimens at the end of the bulging test. It can be seen that the total length of tubes before and after bulging tests has almost no change by observation. This phenomenon is verified by actual measurements for all tubular specimens after deformation, which means that the tube ends are fixed by the locking system on the machine, so there is no slippage between specimens and die sets during the deformation. Therefore, clear boundary

Table 1 Chemical compositions of tested 5049-O aluminum alloy tubes.

Element	Content (wt%)
Fe	0.154
Si	0.071
Cu	0.004
Mg	1.87
Mn	0.72
Zn	0.015
Ti	0.007
Cr	0.009

Fig. 8 Locking system for ends of tubular specimens on machine.

Table 2 Selected experimental results from tube hydraulic bulge test.

Specimen No.	Pressure (MPa)	Diameter (mm)	Pole thickness (mm)
1	2.0	50.09	1.085
2	4.0	50.28	1.078
3	6.0	51.05	1.063
4	6.6	51.78	1.055
5	7.0	52.35	1.041
6	7.4	52.87	1.024

Fig. 9 Tubular specimens before and after hydraulic test.

conditions that tubes are bulged under a bi-axial stress state can be achieved, and the interface friction between tools and parts can be neglected in analytical or numerical models.

Based on this bulge test data, the inverse identification of tubular material parameters is performed using the optimization technique developed in Section 3.3. Several different sets of starting points in a feasible region are tested in this inverse analysis. The determined optimum parameters, the corresponding gradient of the cost function to design variables, and the error between experimental and computed data at optimum points are presented in Table 3. As can be seen from Table 3, although the guessed initial values cover a large range sometimes even far from the optimum point where the strength coefficient ranges from 300.00 to 500.00, e-value from 0.20 to 0.40, the final identified material coefficients converge to the same solution. Besides, values of the objective function and their gradients in all cases are reduced to the same level approximately and satisfy the optimality conditions, which illustrates the stability and robustness of the inverse framework.

An iteration process of the objective function and its corresponding gradient for the 5th initial value is plotted and presented in Fig. 10. From Fig. 10, it is possible to conclude that the least square error is reduced to a small value close to zero after 5 iterations, which leads to a satisfied fitting quality between experimental and computed data. At the same time, the gradient of the cost function reaches a lower value than the one defined in the stopping criteria and terminates the optimization process. Fig. 11 illustrates the evolution process of material constitutive parameters during the optimization. For design variables, the hardening exponent sharply increases from the initial 0.200 to 0.302 after 1 iteration while remaining the same value at the 2nd iteration and then increasing and reaching the optimum value in next iterations. The strength coefficient has a gradual rise from the initial 300.00 to 379.01 as the number of iterations increases. Only 5 iterations are needed to perform in this framework, and the small number of iterations shows the efficiency of the developed optimization technique to solve the inverse problem.

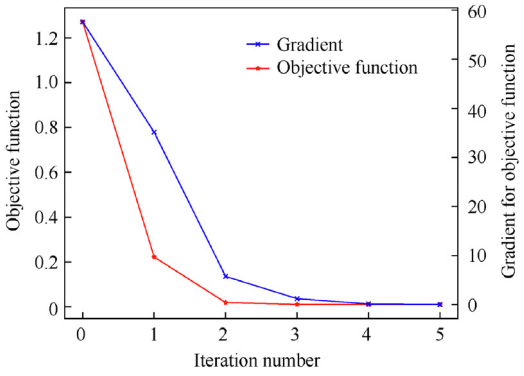

Fig. 10 Iteration process of objective function and its gradient during optimization.

The experimental data obtained from the tube bulge test is imported into the total strain model and Hwang model, and several pairs of points in the strain–stress curve are determined. Fitting these points to the material hardening model defined in Eq. (25) using a least square method, the material strength coefficient and hardening exponent are obtained. As a comparison, material parameters identified by the inverse strategy and two different analytical models are shown in Table 4, and the corresponding flow stress curves can be obtained as shown in Fig. 12.

The strain–stress relationship determined by the universal tensile test is plotted and displayed in Fig. 12. It can be seen from the comparison that there are some differences between the flow stress curve determined by tensile tests and that by hydro bulge tests. The effective stress obtained by bulge tests is lower than that determined by tensile tests, especially at large plastic effective strains. Moreover, a tensile test under a uniaxial stress state overestimates the material deformation limit under a bi-axial tensile stress state when compared with a bulge test. For fitted strain–stress curves based on bulging

Table 3 Identified optimal values for several sets of different initial points.

Set	Initial point $\boldsymbol{x}_0$				Optimum solution $\boldsymbol{x}^*$			
	K	e	$f(\boldsymbol{x}_0)$	$f'(\boldsymbol{x}_0)$	K	e	$f(\boldsymbol{x}^*)$	$f'(\boldsymbol{x}^*)$
1	500.00	0.40	6.43×10^{-2}	1.89	380.88	0.312	9.99×10^{-3}	6.00×10^{-2}
2	450.00	0.35	1.91×10^{-1}	1.66×10^{1}	378.88	0.310	9.95×10^{-3}	5.22×10^{-2}
3	400.00	0.30	5.08×10^{-1}	3.01×10^{1}	379.07	0.310	9.96×10^{-3}	9.64×10^{-2}
4	350.00	0.25	9.16×10^{-1}	4.30×10^{1}	379.15	0.310	9.96×10^{-3}	8.83×10^{-2}
5	300.00	0.20	1.27	5.76×10^{1}	379.01	0.310	9.96×10^{-3}	6.61×10^{-2}
6	300.00	0.40	5.23×10^{3}	1.30×10^{5}	379.04	0.310	9.95×10^{-3}	7.32×10^{-2}
7	350.00	0.35	1.55×10^{1}	7.58×10^{2}	378.73	0.310	9.96×10^{-3}	1.04×10^{-1}
8	450.00	0.30	1.63	3.50×10^{1}	379.89	0.311	9.97×10^{-3}	5.77×10^{-2}
9	500.00	0.25	3.38	2.62×10^{1}	379.30	0.310	9.96×10^{-3}	8.21×10^{-2}
Mean value					379.33	0.310		

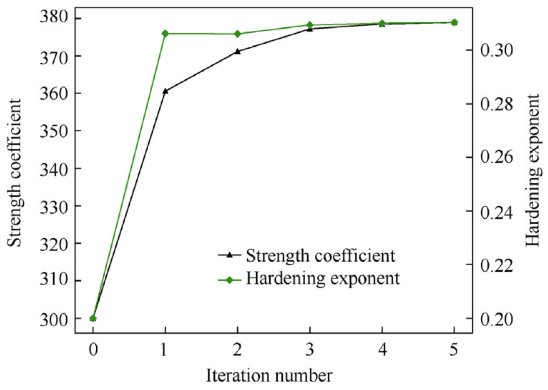

Fig. 11 Iteration process of design variables during optimization.

Table 4 Identified flow stress models using different methods.

Testing method	Model	Strain–stress relation
Tensile test		$\sigma = 396.75\varepsilon^{0.297}$
Bulge test	Inverse	$\sigma = 379.33\varepsilon^{0.310}$
	Hwang	$\sigma = 418.08\varepsilon^{0.366}$
	Total strain	$\sigma = 433.16\varepsilon^{0.362}$

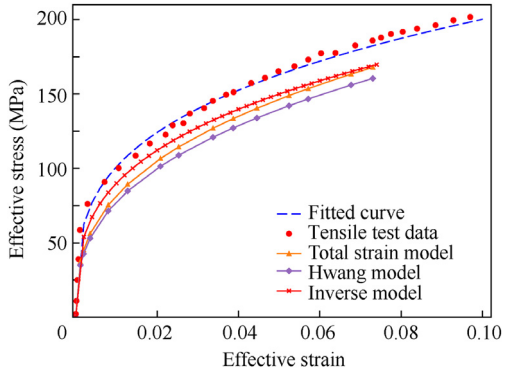

Fig. 12 Comparison of effective strain–stress curves obtained by tensile test and bulge test.

tests, three models give identical results of tensile tests in the small strain region, and the stress difference raises with an increase of the strain. The effective stress predicted by Hwang model is always lower than those by the other two models. Then the flow stress curve determined by the inverse model is very close to that by the total strain model in a large strain range, while the difference between the results of the inverse model and the tensile test is smaller compared with those of the other two analytical models.

In order to evaluate the performance of different tests and models, FEM simulations for the tube hydraulic bulging process are performed by LS-DYNA program with identified flow stress curves. Other input data like the pressure loading curve and simulation speed are identical in numerical models. The calculated pole thickness, bulge height, and profile shape in the deformation zone are analyzed and compared with those from the physical experiment.

Fig. 13 shows the comparison of the internal pressure versus the bulge height curves between experimental data and numerical outputs of FEM models using material parameters given in Table 4. It can be seen that the calculated bulge height with a flow curve identified by the inverse model has a good agreement with the experimental data when compared with the other three methods. Furthermore, a detailed quantitative deviation is displayed in Table 5 and Fig. 14. It is demonstrated that the relative deviations between simulation results of all methods and experimental measurements are higher at lower bulging pressures, while these deviations are reduced as the pressure increases. Furthermore, the smallest mean value of the relative deviation also validates that material parameters obtained by the inverse model are more accurate than those by Hwang and total strain models.

Fig. 15 shows the comparison of the internal pressure versus the pole thickness curve between experimental data and the corresponding FEM results using various flow stress curves. Fig. 16 and Table 5 illustrate a quantitative error comparison and analysis. As can be seen from these results, material parameters determined by inverse model lead to satisfactory fitting agreement and the smallest mean deviation between experimental and numerical data. A higher relative deviation is observed at high bulging pressure levels for Hwang model and tensile tests. For the total strain and inverse models, the small deviation is still kept throughout the deformation process, especially for the inverse model which performs better than other models at a large-deformation state.

The calculated bulge profile using constitutive parameters determined by different models can be observed in Fig. 17, in which the measured tube radii along longitudinal positions in experiments are presented. It is obvious that the predicted bulge profile based on the tube bulge test matches better to experimental measures compared with that of the tensile test. The quantitative gap between experimental data and FEM outputs by three models can be observed in Fig. 18 and Table 5, and it can be seen that the bulge profile calculated by the inverse model leads to the smallest deviation and is very close to experimental results compared with those of Hwang and total strain models.

From these comparisons, it can be concluded that the three models, i.e. the inverse model, the total strain model, and

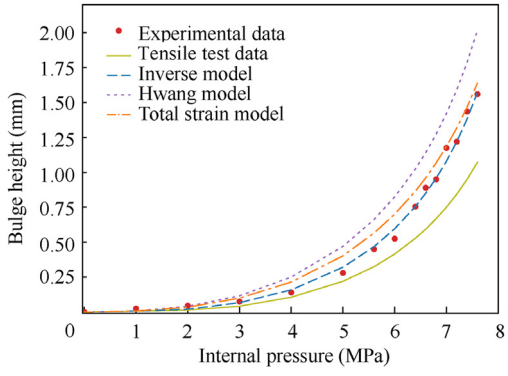

Fig. 13 Comparison of internal pressure versus bulge height curves obtained by different methods.

Table 5 Relative deviations between simulation data and experimental measured results.

Data type	Test method and model	Relative deviation (%)		
		Min	Mean	Max
Bulge height	Inverse model	5.74×10^{-4}	1.44×10^{-1}	7.18×10^{-1}
	Hwang model	9.66×10^{-2}	4.21×10^{-1}	7.89×10^{-1}
	Total strain model	8.63×10^{-3}	2.39×10^{-1}	7.17×10^{-1}
	Tensile test	2.09×10^{-1}	3.60×10^{-1}	7.20×10^{-1}
Pole thickness	Inverse model	1.73×10^{-4}	1.48×10^{-3}	4.41×10^{-3}
	Hwang model	1.66×10^{-4}	8.48×10^{-3}	1.58×10^{-2}
	Total strain model	8.30×10^{-5}	3.15×10^{-3}	8.35×10^{-3}
	Tensile test	2.30×10^{-4}	7.81×10^{-3}	2.18×10^{-2}
Bulge profile	Inverse model	3.79×10^{-4}	1.58×10^{-3}	3.04×10^{-3}
	Hwang model	7.33×10^{-3}	1.26×10^{-2}	1.80×10^{-2}
	Total strain model	3.18×10^{-3}	3.52×10^{-3}	5.01×10^{-3}
	Tensile test	6.12×10^{-3}	1.20×10^{-2}	1.76×10^{-2}

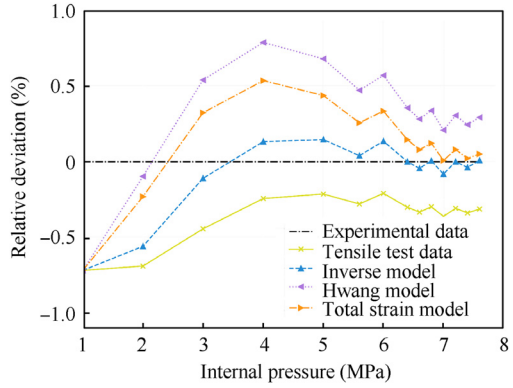

Fig. 14 Deviation analysis of internal pressure versus bulge height curves obtained by different methods.

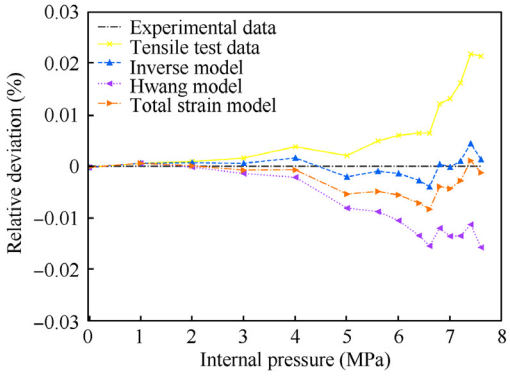

Fig. 16 Deviation analysis of internal pressure versus pole thickness curves obtained by different methods.

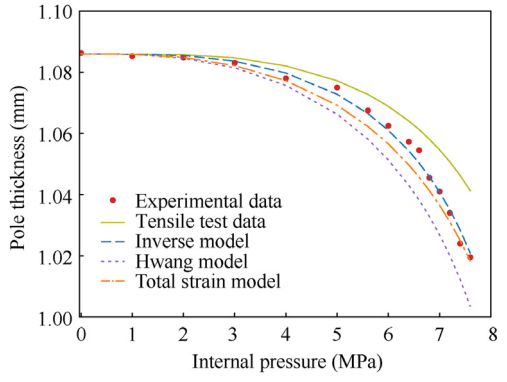

Fig. 15 Comparison of internal pressure versus pole thickness curves obtained by different methods.

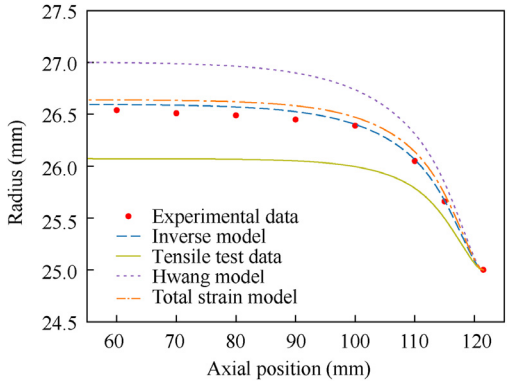

Fig. 17 Comparison of axial position versus bulge profile obtained by different methods.

Hwang model, can be used to translate the collected experimental data into a flow stress curve, while the inverse model presents more satisfying results to experimental measures compared with those of the other two models. One reason for that is the inverse model removes the geometrical and mechanical assumptions in analytical models, and the isolated analysis of the stress and strain in Hwang model and assumptions in the total strain model lead to a big difference between simulated and experimental data.

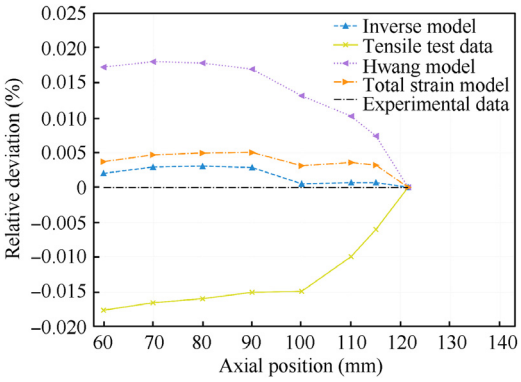

Fig. 18 Deviation analysis of axial position versus bulge profile obtained by different methods.

6. Conclusions

(1) Tube bulging tests with fixed-end conditions for 5049-O aluminium alloy are performed on a flexible hydraulic forming press. The bulge height, pole thickness, and bulge profile under different fluid pressure levels are measured during experiments.

(2) An inverse framework combining the incremental strain theory with an improved Levenberg-Marquardt algorithm is developed to identify tubular metal properties by a minimization of the least square error between calculated and experimental data. Several sets of initial guesses are tested for this inverse strategy, and the convergence to an identical optimum solution shows that this framework is robust and efficient for characterization of tubular materials.

(3) Two analytical models based on membrane mechanics and the total strain theory are proposed to model the hydro bulging process and determine the strain–stress relationship of 5049-0 aluminium alloy. Obtained flow stress curves are compared with that from a tensile test, which demonstrates that a bulge test is more suited to characterize the tubular material behavior because its stress state is closer to the actual hydroforming process.

(4) FEM simulations for a free bulge test are conducted using identified flow stress curves from different tests and models. Predicted bulge height, bulge profile shape, and pole thickness from FEM models are compared with measured values, and results from the inverse model show a good agreement with experimental data. It can be concluded that the inverse model is more accurate than Hwang and total strain models for characterization of tubular material properties.

Declaration of Competing Interest

The authors declare that they have no known competing financial interests or personal relationships that could have appeared to influence the work reported in this paper.

Acknowledgement

The first author acknowledges the financial support from China Scholarship Council (CSC) (No. 201706080020) for his study at Aalborg University in Denmark.

Data availability statement

The raw data required to reproduce these findings are available from the corresponding author upon reasonable request.

References

1. Wang Y, Lang L, Sherkatghanad E, et al. Design of an innovative multi-stage forming process for a complex aeronautical thin-walled part with very small radii. *Chin J Aeronaut* 2018;**31**(11):2165–75.
2. Zhan M, Guo K, Yang H. Advances and trends in plastic forming technologies for welded tubes. *Chin J Aeronaut* 2016;**29**(2):305–15.
3. Alaswad A, Benyounis KY, Olabi AG. Tube hydroforming process: A reference guide. *Mater Des* 2012;**33**:328–39.
4. Bruschi S, Altan T, Banabic D, et al. Testing and modelling of material behaviour and formability in sheet metal forming. *CIRP Ann* 2014;**63**(2):727–49.
5. ASTM E8/E8M-21. *Standard test methods for tension testing of metallic materials*. West Conshohocken: ASTM International; 2021.
6. Wang H, Martin P. Tube formability assessment for tube hydroforming. *SAE Int J Mater Manuf* 2002;**111**(5):880–9.
7. Fuchizawa S, Narazaki, Yuki H. Bulge test for determining stress-strain characteristics of thin tubes. In: Wang ZR, He YX, editors. *Advanced technology of plasticity. Proceedings of the 4th international conference on technology of plasticity;* 1993 Sep 5–9; Beijing, China. Beijing: International Academic Publishers; 1993. p. 488–93.
8. Hwang YM, Lin YK, Altan T. Evaluation of tubular materials by a hydraulic bulge test. *Int J Mach Tools Manuf* 2007;**47**(2):343–51.
9. Velasco R, Boudeau N. Tube bulging test: Theoretical analysis and numerical validation. *J Mater Process Technol* 2008;**205**(1-3):51–9.
10. Ynag LF, Guo C. Determination of stress-strain relationship of tubular material with hydraulic bulge test. *Thin Walled Struct* 2008;**46**(2):147–54.
11. Bortot P, Ceretti E, Giardini C. The determination of flow stress of tubular material for hydroforming applications. *J Mater Process Technol* 2008;**203**(1–3):381–8.
12. Ponthot JP, Kleinermann JP. A cascade optimization methodology for automatic parameter identification and shape/process optimization in metal forming simulation. *Comput Methods Appl Mech Eng* 2006;**195**(41–43):5472–508.
13. Cho H, Altan T. Determination of flow stress and interface friction at elevated temperatures by inverse analysis technique. *J Mater Process Technol* 2005;**170**(1-2):64–70.
14. Andrade-Campos A, Thuillier S, Pilvin P, et al. On the determination of material parameters for internal variable thermoelastic-viscoplastic constitutive models. *Int J Plast* 2007;**23**(8):1349–79.
15. de-Carvalho R, Valente RAF, Andrade-Campos A. Optimization strategies for non-linear material parameters identification in metal forming problems. *Comput Struct* 2011;**89**(1-2):246–55.
16. Shrot A, Bäker M. A study of non-uniqueness during the inverse identification of material parameters. In: Wegener K, editor. *CIRP: Proceedings of 5th CIRP Conference on high performance cutting;* 2012 Jun 4–7; Zürich, Switzerland. New York: Curran; 2012. p. 72–7.
17. Rauchs G, Bardon J. Identification of elasto-viscoplastic material parameters by indentation testing and combined finite element modelling and numerical optimization. *Finite Elem Anal Des* 2011;**47**(7):653–67.
18. Zribi T, Khalfallah A, BelHadjSalah H. Experimental characterization and inverse constitutive parameters identification of tubular materials for tube hydroforming process. *Mater Des* 2013;**49**:866–77.

19. Khalfallah A, Oliveira MC, Alves JL, et al. Mechanical characterization and constitutive parameter identification of anisotropic tubular materials for hydroforming applications. *Int J Mech Sci* 2015;**104**:91–103.
20. He ZB, Yuan SJ, Lin YL, et al. Analytical model for tube hydrobulging test, Part I: Models for stress components and bulging zone profile. *Int J Mech Sci* 2014;**87**:297–306.
21. Song WJ, Kim J, Kang BS. Experimental and analytical evaluation on flow stress of tubular material for tube hydroforming simulation. *J Mater Process Technol* 2007;**191**(1-3):368–71.
22. Ilyushin AA, Lensky VS. *Strength of materials*. Oxford: Pergamon Press; 1967. p. 199–207.
23. Andrade-Campos A, de-Carvalho R, Valente RAF. Novel criteria for determination of material model parameters. *Int J Mech Sci* 2012;**54**(1):294–305.
24. Cao J, Lin J. A study on formulation of objective functions for determining material models. *Int J Mech Sci* 2008;**50**(2):193–204.
25. Nielsen HB. Damping parameter in Marquardt's method. Lyngby: Technical University of Denmark; 1999. Report No.: IMM-REP-1999-05.
26. Moré JJ. The Levenberg-Marquardt algorithm: Implementation and theory. In: Watson GA, editor. *Numerical analysis. Proceedings of the biennial conference;* 1977 Jun 28–Jul 1; Dundee, Scotland. Berlin: Springer; 1978. p. 5–16.